January, 2005
CERN/SPSC 2005-001
SPSC-M-728

Atomic Spectroscopy and Collisions Using Slow Antiprotons

ASACUSA Collaboration

2004 Status Report

Contents

1 PPB-scale laser spectroscopy of $\overline{p}\mathrm{He}^+$ atoms

In 2002, we used the radio-frequency quadrupole decelerator (RFQD) to stop 100-keV antiprotons in a low density helium gas target ($10^{16} - 10^{18}$ cm^{-3}, about a factor 1000 to 100,000 lower than in ASACUSA Phase 1 measurements). This completely eliminated the collisional shifts and widths of the laser resonance lines, making it possible to measure 13 $\overline{p}\mathrm{He}^+$ laser resonances to $\sim$ 100-ppb-precision each[1], and to extract the best baryonic CPT limits of $\delta_{\bar{p}} = (Q_p + Q_{\bar{p}})/Q_p = (M_p - M_{\bar{p}})/M_p = 10$ ppb (10^{-8}) [2], where $Q_{p(\bar{p})}$ and $M_{p(\bar{p})}$ respectively are the proton (antiproton) charge and mass.

In 2004, we measured the transition frequencies of $\overline{p}\mathrm{He}^+$ (twelve transitions shown in Fig. 1, seven in $\bar{p}^4\mathrm{He}^+$ and five in $\bar{p}^3\mathrm{He}^+$) to about a factor 10 better than our 2002 measurements,

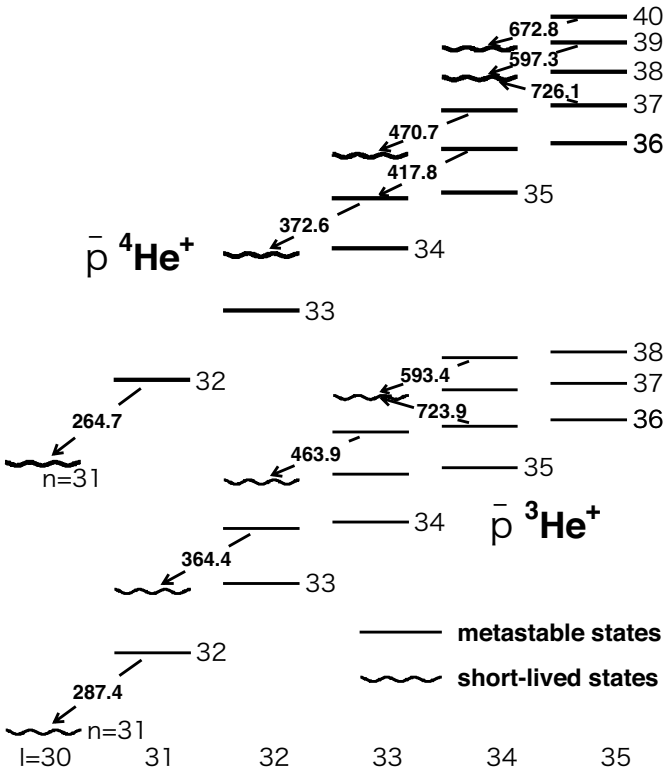

Figure 1: In 2004, seven transitions in $\overline{p}^4\mathrm{He}^+$ and five in $\overline{p}^3\mathrm{He}^+$ were measured using the pulse-amplified single-mode CW laser.

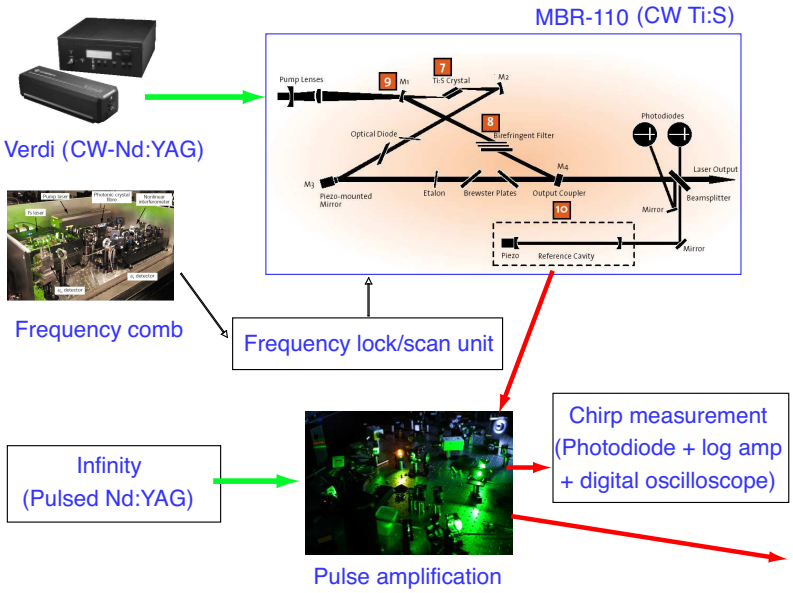

Figure 2: Schematic layout of the high-precision laser system used in 2004.

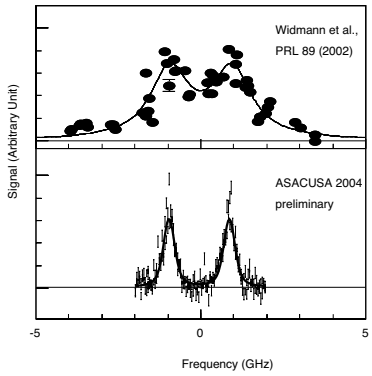

Figure 3: Comparison of the laser scans over the 726-nm resonance with the commercial pulsed dye laser (top) and the pulse-amplified single-line mode CW laser (bottom). The clear separation of the hyperfine doublet (separation 1.8 GHz) is achieved in 2004.

using a constant-wave pulse-amplified laser and a femtosecond optical-frequency comb generator [3, 4], schematically depicted in Fig. 2. The data are being evaluated and will be compared with revised theoretical values; with the 2004 data, the proton-antiproton mass (charge) comparison is likely to be improved to ~ 1 ppb.

Table 1 shows various factors limiting the experimental accuracy and precision of $\overline{p}\mathrm{He}^+$ laser spectroscopy. Of these, the first two (collisional effects) had been taken care of already by the RFQD. Let us briefly discuss other improvements made in 2004 (points [1]–[5] of Table 1) in the following:

[1] So far, our 'instrumental resolution' was dominated by the bandwidth of a commercial pulse dye laser. Each laser pulse contained several 'modes', whose relative intensities fluctuated from shot to shot[5]. Instead, in 2004, we used a constant-wave, single-line mode titanium sapphire or dye laser with a frequency bandwidth $\delta f/f < 10^{-10}$, and a pulse amplifier which converted the CW laser light into high-energy pulses with peak powers of 0.1–1 gigawatt. Fig. 3 demonstrates the resolution improvement achieved in 2004.

[2] The *frequencies* (instead of wavelengths) of the single-line-mode CW lasers were measured

Table 1: Various factors limiting the experimental accuracy and precision of $\overline{p}\mathrm{He}^+$ laser spectroscopy.

	ASACUSA Phase 1 (2000)	Phase 2 (2002)	2004	Note (see text)
Collisional shift	~ 500 MHz	$\sim$ MHz	$\leftarrow$	
Collisional width	~ 500 MHz	$\sim$ MHz	$\leftarrow$	
Laser bandwidth	~ 2000 MHz	~ 800 MHz	< 20 MHz	[1]
Laser calibration	10–60 MHz	$\leftarrow$	~ 1 MHz	[2]
Chirp	not measured	$\leftarrow$	corrected to ~ 1 MHz	[3]
Fourier limit	~ 100 MHz	$\leftarrow$	~ 10 MHz	[4]
Natural width	0.1 – 100,000 MHz	$\leftarrow$	$\leftarrow$	[5]
Doppler width	~ 500 MHz	$\leftarrow$	$\leftarrow$	

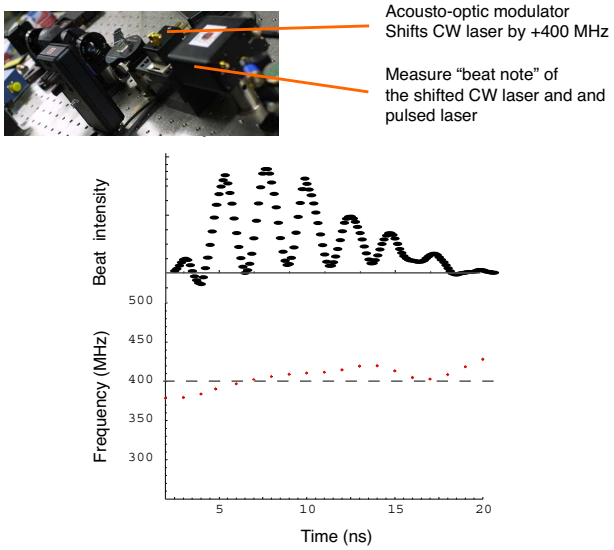

Figure 4: Chirp correction.

with a femtosecond optical comb generator with a relative accuracy of $\sim 10^{-12}$. The CW lasers were locked to the comb generator, and their frequencies were swept across the $\overline{p}\mathrm{He}^{+}$ laser resonance lines.

[3] Even though the frequency of the CW laser is accurately measured using the comb generator, the laser frequency after the pulse-amplification stage is in general different from the input CW frequency. This effect is called the 'chirp'. We used an active chirp compensation scheme using an electro-optic modulator. In addition, in order to measure the chirp effect and to correct for the frequency shift, we measured for each laser shot a beat note between a 400-MHz-shifted CW laser and the output of the pulse amplifier (see Fig. 4), both systems being similar to the ones used in the muonium 1S-2S laser spectroscopy[6]. As shown in Fig. 4, the Fourier analysis of the beat intensity reveals some ± 20 MHz walk of the laser frequency during the 20-ns laser pulse. In our final results, the uncertainty due to the chirp is expected to be reduced to ~ 1 MHz, as was achieved for the muonium case[6].

[4] The pulse width τ_w of the Nd:Yag pump laser was expanded with an optical delay line by about a factor 10 to $\tau_w \sim 20$ ns, so as to improve the Fourier limit $(1/(2\pi\tau_w))$.

[5] One of the twelve transitions we measured, $(n, l) = (36, 34) \rightarrow (35, 33)$ at 417.8 nm is a metastable-to-metastable transition. The transitions we have so far measured to high precision are metastable-to-short-lived (see Fig. 1), *i.e.,* the lifetime of the parent state is $\sim 1\mu$s while that of the daughter state is < 10 ns. Of course the natural linewidths ($\Gamma_{\mathrm{nat.}}$ ~10 MHz – 100 GHz) can be a limiting factor, but we are more concerned with theoretical accuracies. The accuracies of the three-body QED calculations[7, 8] are supposedly higher for those transitions having smaller widths ($\Delta\nu_{\mathrm{theory}} \sim \Gamma_{\mathrm{nat.}}/100$[7]). We thus took high-statistics data for the 417.8 nm transition using a double-resonance technique (use two lasers, one tuned to the 417.8 nm transition and the other tuned to the 372.6-nm transition).

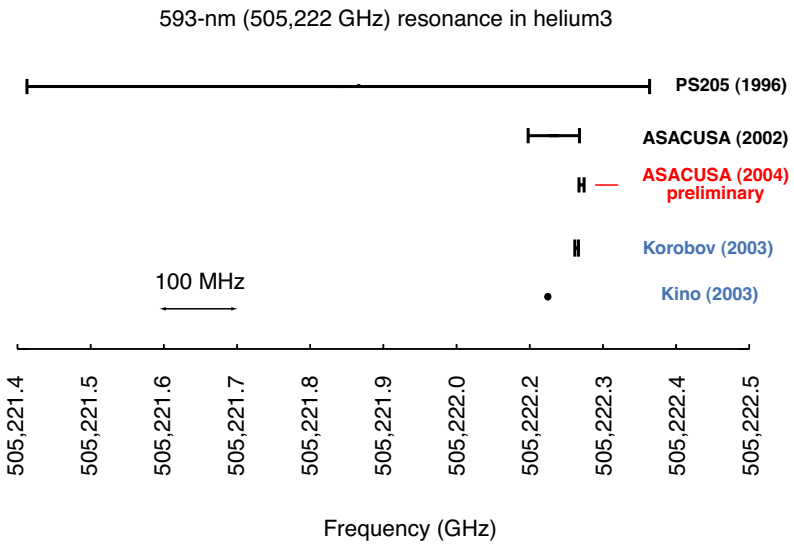

Figure 5: A preliminary 2004 result for the 593-nm transition in $\bar{p}^3\mathrm{He}^+$ is compared with our previous measurements and two theoretical values.

In Fig. 5, we compare the central frequency for the 593-nm transition in $\bar{p}^3\mathrm{He}^+$ measured in 2004 (preliminary) with that of two previous measurements (one at LEAR (PS205)[9] and the other at AD with the RFQD[1]), and two theoretical values[7, 8]. As shown, our new value has a much smaller error bar, and clearly favors one of the two theoretical calculations.

So far, experimental errors[1] and scatter of theoretical numbers[7, 8] have been all about 100 ppb. With our 2004 results, the differences between the two sets of calculations have become the dominant error source when we deduce the proton-antiproton mass (and charge) CPT limits. Both of the theoretical calculations are being updated, and the preliminary results are encouraging.

When we finish analyzing our data and theorists finish updating the predictions, we hope to be able to determine antiproton mass to ~ 1 ppb. This is close to the present precision of the electron-proton mass ratio of 0.46 ppb[10] (note that the proton-to-electron mass ratio has moved by 2.8 ppb between CODATA98 and CODATA02 compilations, see Fig. 6).

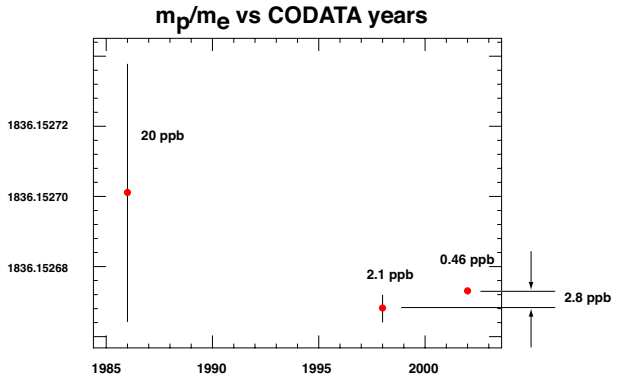

Figure 6: CODATA values of m_p/m_e.

Table 1 shows that the largest remaining factor contributing to the line width (and hence precision) is the Doppler effect, and precision higher than $\sim$ 1 ppb may be reached if we can eliminate the Doppler width. A plan for a Doppler-free spectroscopy is presented in 'addendum to ASACUSA'.

2 Successful extraction of an ultra-slow antiproton beam in great numbers

ASACUSA has succeeded this year in producing an ultra-slow monoenergetic antiproton beam by sequentially combining the beams from the AD (down to 5.3 MeV), the RFQD (Radio-Frequency Quadrupole Decelerator; down to 50–120 keV), and confining them in a MRT (multi-ring electrode trap) installed in a superconducting magnet of 2.5 T. Here they are cooled and compressed before being extracted, re-accelerated to eV-scale energies and delivered via a beam transport line to gas or solid targets. The MRT, the superconducting solenoid and eV-beam transport line are jointly known as "MUSASHI", or the Monoenergetic Ultra-Slow Antiproton Source for High-precision Investigations. MUSASHI opens a new research field of collision dynamics to be studied in processes like antiprotonic atom formation and ionization processes under 'single collision conditions'.

During 2004, we succeeded in extracting a large number of antiprotons from the trap. Among 1 million antiprotons trapped at a single AD shot and then cooled, more than 60% were extracted out of the strong magnetic field, more than 500,000 antiprotons were detected by an MCP (microchannel plate) placed 170 cm from the trap center, and 300,000 antiprotons were successfully transported at an energy as low as 250 eV until the end of our extraction beamline of 3 m, after having passed through three apertures, each time refocused by a set of electric Einzel lenses. This success is a great leap from the previous year's situation where only 60,000 antiprotons at maximum were counted by the MCP, only 4,000 out of them being transported until the very end. The ultra-low energy antiprotons were extracted continuously during a period of up to 10 s, and this length should be easily expanded if needed. A variety of physics experiments will become possible using this unique beam, ranging from atomic physics to nuclear physics. The ultra-low energy of the beam allows single collision experiment with atomic targets, while the slow extraction *i.e.* the continuous aspect of the beam allows event-by-event data acquisition associated with each single antiproton extracted, which were not possible with the direct beam from the AD facility or out of the RFQD, extracted in a pulsed mode.

2.1 Status until 2003

Until 2003, we were troubled by the problem that most of the one million antiprotons trapped and cooled in the MRT hit an extractor electrode 70 cm downstream, where the magnetic field was 10–20% of the value 2.5 T at the center (see Fig. 7). This meant that the antiproton cloud had a diameter of 15–20 mm in the trap. In order for the cooled antiprotons to be transported well enough until the end of our extraction beamline of 3 m length after the superconducting solenoid, the radial blow-up of the antiproton beam should be limited to less than 4 cm in diameter just before the first Einzel lens located 130 cm downstream of the MRT, where the magnetic field was several milliteslas. To fulfill this condition, the antiproton cloud in the trap at 2.5 T had to have a diameter less than 2 mm, as was shown by our simulation. Clearly we needed a breakthrough in dramatic compression of the antiproton cloud in the trap.

2.2 Movable electron gun

Antiprotons injected into the strong magnetic field and captured in the MRT were cooled by preloaded electrons injected from downstream. The electron gun was mounted outside a cylindrical extractor electrode, in order to keep axial symmetry of the electric field and not to conflict with the passage of low-energy antiproton beams to be extracted downstream. Thus the electrons emitted from the Spindt-type field-emission electron gun were guided along the converging magnetic field line into the electrode across a mesh attached on a side slit. With this configuration, however, the electron plasma formed consequently had a diameter of 1 cm or more. Since the antiprotons were confined in the harmonic potential after having lost most of its incident energy of up to 10 keV by collision with the electrons, control of the size of the electron plasma was an important key in obtaining an antiproton cloud compressed within a small enough diameter. We therefore modified the system so that the electron gun should be translationally movable into the extraction electrode. This allowed the electrons to be introduced along the central axis into the MRT before antiproton injection and to form a spheroidal plasma with a small enough diameter, while the plate mounting the electron gun can be pulled out before extraction of the antiprotons.

2.3 Alignment of the bore

Alignment of three axes, namely the magnetic axis, axis of the MRT, antiproton injection and extraction axes needed to be adjusted precisely. Especially, even a slight misalignment between the magnetic axis and the MRT axis, *i.e.* the electric axis can cause radial expansion and loss of the electron plasma and the antiproton cloud. We found out, that this alignment was not necessary well enough tuned until the year 2003. After the modification of the electron gun, it became possible to use an anode plate at the central axis as a Faraday cup to collect electrons when they were extracted downstream for diagnostic purpose. Since any misalignment of the bore tube which housed the MRT electrodes would result in a large displacement of the extracted electron beam outside the strong magnetic field, the collection efficiency by the anode plate can give a sensitive reference of the alignment.

Density and aspect ratio of the electron plasma were diagnosed from a series of measurements of the plasma excitation modes using the technique developed in 2003 [11, 12]. The size of the electron plasma can now be deduced unambiguously from combination of these plasma parameters and the total charge which newly became measurable by the Faraday cup.

The optimum bore position was searched where the electron plasma had a smallest diameter and also the extracted electrons were collected with the highest efficiency. After a long series of these alignment procedures, we finally found that the optimum position was as much as 2 mm off from the assumed geometrical center both horizontally and vertically. At this position, electrons were stably stored in the MRT, in numbers of 3×10^8 with a plasma diameter of 1–2 mm.

2.4 Decompression of electron plasma

Antiproton beam transport, extracted from AD at 5.3 MeV and then decelerated to 111 keV by the RFQD and injected into the MRT in the 2.5 T magnetic field, was tuned with great care, sometimes spending a major fraction of our share of the beamtime. The two-dimensional position and distribution of the 111 keV beam at the LEBT (Low-Energy Beam Transport) section was monitored by two sets of microwire secondary emission chambers and by a thin-strip detector evaporated onto a degrader foil which decelerated the antiproton beam further down to less than 10 keV in the 2.5 T magnetic field. The radial distribution of the antiproton

beam had a diameter of 3–4 mm FWHM under the best beam tuning conditions. In order for the electron plasma to cover the distribution of antiprotons and cool them effectively, the plasma was radially expanded before antiproton injection, to 4–7 mm in diameter. (Note that the electron plasma has a sharp-cut radial density distribution.) To do this, a rotating electric field was applied across one of the trapping electrodes azimuthally split into 4 segments, at a frequency swept from 500 kHz to 3 MHz over a period of 30–60 s. This process, known as rotational (de)compression of the plasma, was also tried before, but was not effective until the year 2004. Now that the bore is perfectly aligned, we have reliable control and diagnosis of the electron plasma and of the antiproton cloud.

2.5 Cooling, compression and extraction of antiprotons

After the antiprotons were effectively cooled by the electrons and trapped in the harmonic potential of 50 eV depth, the electrons needed to be removed out of the same potential, because their continued presence caused antiproton losses during the subsequent extraction procedures. To do this one wall of the potential well was lowered several times for a period of 550 ns. This was long enough for the electrons to escape while the much heavier, slower antiprotons were scarcely affected. The antiproton cloud was then radially compressed by a rotating wall field at 250 kHz for 120–400 s, before extraction when the harmonic potential was ramped gradually over a period of typically 40 s. The antiprotons were accelerated and were transported along the beamline at 250 eV. The beam was electrically refocused three times by sets of Einzel lenses, passing through three apertures placed at the focal positions, as is shown in Fig. 7 [13]. These variable apertures of diameter 4–10 mm enabled differential pumping of 6 orders of magnitude of vacuum, in order to keep the ultra-high vacuum inside the MRT ($< 10^{-12}$ Torr) when a gas-target of 10^{-6} Torr was used at the end of the beamline for collision experiments mentioned in the following section.

Annihilation of antiprotons along the extraction beamline was detected by a pair of scintillator bars near and parallel to the track axis. Readout of these by PM tubes at both ends allowed the z-position of annihilation vertices to be reconstructed. Without rotation, most of the antiprotons radially expanded drastically enough to hit the extractor electrodes in the middle of the beamline. When the rotating wall field was applied, we observed that some of the distribution shifted downstream. Figure 8 shows histograms of the annihilation position for different periods of field application, under the condition that one of the three gate valves, GV2, was kept closed. It shows that the longer time the rotation was applied, the more effectively was the main part of the antiproton beam transported toward downstream until the position of the closed gate valve. This series of data is a clear evidence of effective radial compression of the antiproton cloud.

We then opened GV2, fine tuned the beam transport parameters to confirm that main part of the antiproton beam annihilated at the position of the next gate valve GV3 downstream before we opened it for further transport. This series of observation is summarized in Fig. 9. Here, closed gate valves were opened one by one, to check the annihilation position along the transport beamline. Despite rather poor position resolution, each figure clearly show a main peak at the position of the closed gate valve. The main peak is absent in the last figure, implying that major part of the beam has been successfully transported to the very end of the beamline. Although the track detector solid angles were here very small and their sensitivity was consequently drasically reduced, we could insert MCP2 (Fig. 9) from time to time. Using data from both MCPs jointly with the track detector efficiency we could conclude that more than 500,000 antiprotons were extracted over a period of 10 s as a monoenergetic beam at 250 eV, and 300,000 of them reached

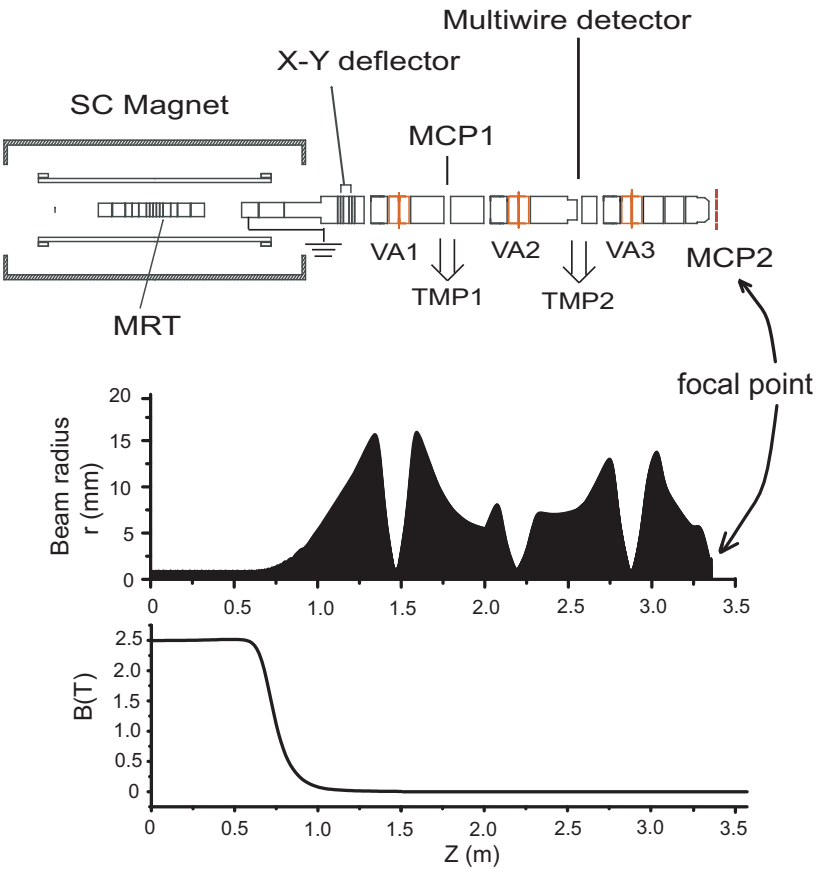

Figure 7: A schematic drawing of the MUSASHI trap (MRT) and the extraction beamline, overlaid with a graph of magnetic field strength and calculated trajectories of the antiproton beam at 250 eV which was focused three times at variable apertures (VA).

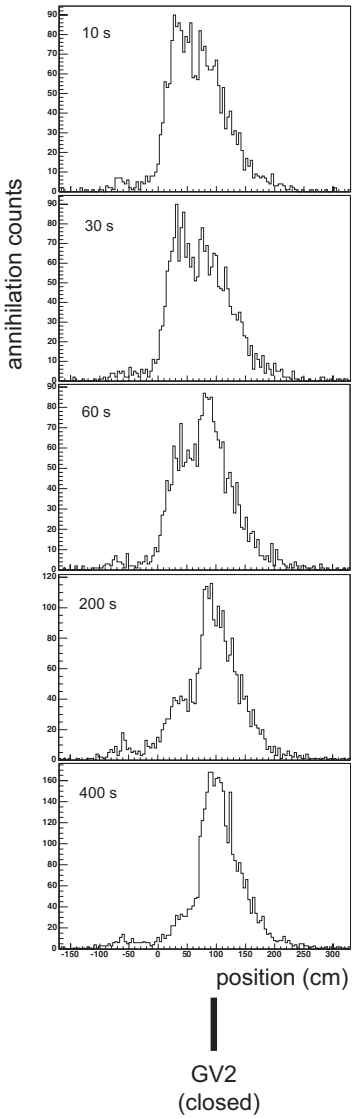

Figure 8: Annihilation position of antiprotons extracted after varied periods of application of the rotating wall field, showing effective compression of the antiproton cloud.

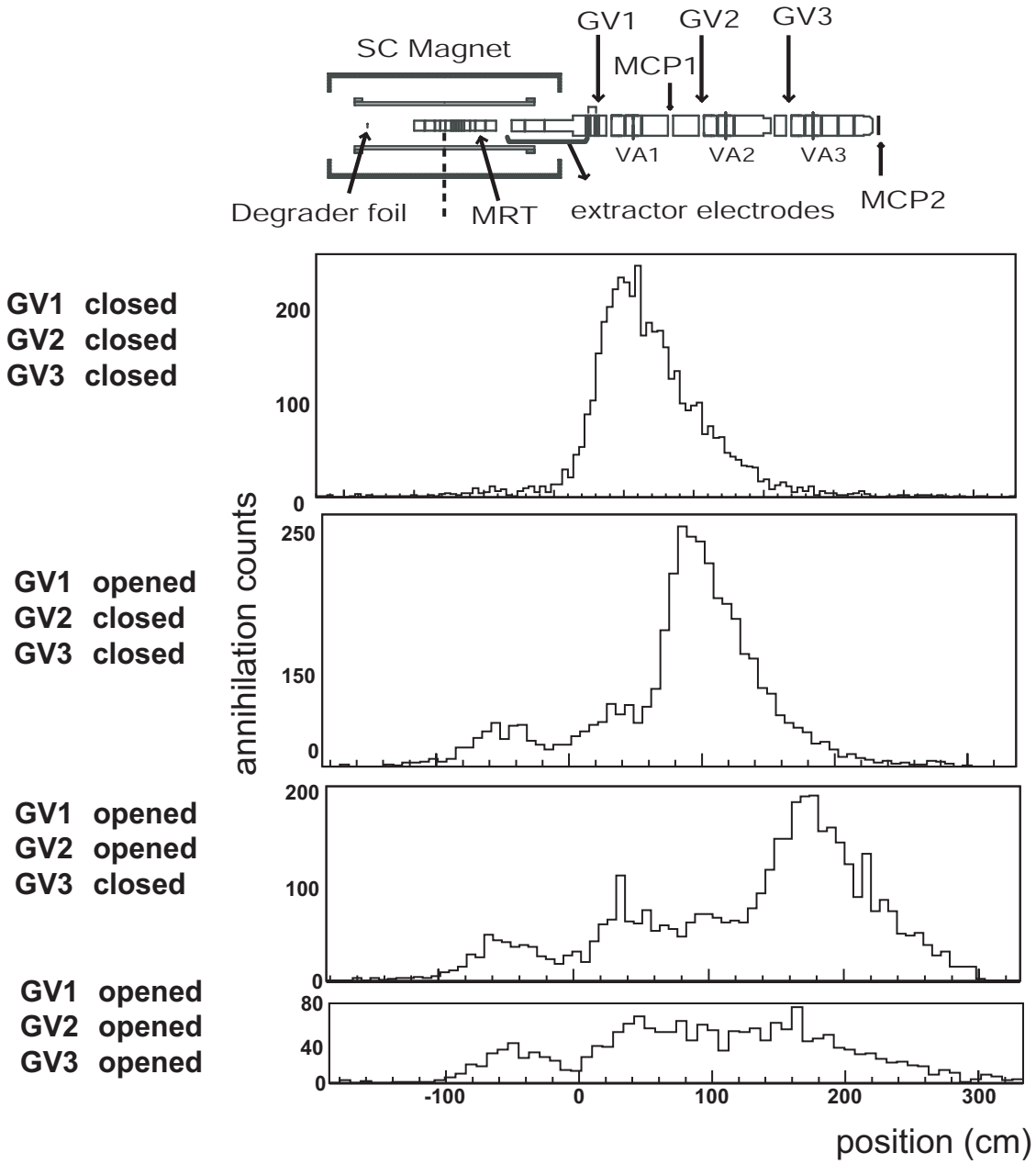

Figure 9: Position distribution of antiproton annihilation along the MUSASHI extraction beamline. The main part of the antiproton beam was transported efficiently before hitting a closed gate valve (GV). In the last figure, absence of the main peak indicates successful beam transport until the end of the beamline at the position of MCP2, where the track detectors had practically no sensitivity.

the end of the 3 m transport beamline.

Due to our limited hours of beamtime during this year, we concentrated our effort in optimizing the beam transport at a fixed energy of 250 eV, but the MUSASHI beamline is designed to transport antiprotons ranging from 10 eV to 1 keV, as was partially demonstrated in previous years. It is also possible to accelerate the beam in a later stage to tens of kilovolts.

2.6 Collision experiments using the ultra-slow antiproton beams

Our success in slow extraction of a large number of antiprotons at ultra-low energy opened up a new field of atomic physics which has so far been inaccessible. As the first physics application, gas-jet targets were prepared for measurement of ionization cross section of atoms by low-energy antiprotons. The apparatus, which was floatable at a variable voltage up to 30 keV, was finally connected at the end of the MUSASHI beamline via another beam transport to allow re-acceleration of the continuous antiproton beam. After some beam tuning, we counted 100,000 antiprotons re-accelerated to 25 keV through two additional apertures. During a few shifts of experiment, the MUSASHI beamline provided 70,000 antiprotons steadily into the target chamber per extraction cycle of 4 minutes, and ionization signals from antiproton – helium atom collision were successfully observed at 25 keV, as will be explained in the following chapter.

We also prepared another set of apparatus of gas-jet targets, aiming at measurement of capture cross section of antiprotonic atoms at 10–1000 eV. We worked on the modification of the target chamber in collaboration with a gas-target specialist and improved the gas density by one order of magnitude. This apparatus was also connected to the beamline in the very last moment, but the experiment could not be performed due to technical problems and lack of our beamtime. These physics programs will be continued in the year 2006 and onward.

3 $\bar{p}$-atom Ionization cross section measurements

3.1 History of experiment and apparatus

The Aarhus Ionization Apparatus (AIA) was originally designed for use with the slow, extracted antiproton beam created by the MUSASHI penning trap. It was anticipated, that we could get slow extraction of antiprotons of ∼eV energy. We therefore designed a classic ionization experiment, depending on the measurement of the TOF for each ion created in an ionizing collision between an antiproton and a target atom.

Figure 10 shows the result, schematically. The target region can be seen as well as the ion and $\bar{p}$ detectors. Also an electron gun can be inserted into the beam axis together with a Faraday cup. This makes possible a measurement of the integrated target density and detector efficiency using keV electron beams and tabulated electron cross sections. Furthermore, a polyoxymethylene (POM) insulator is seen. This is meant to make it possible to raise the target region to high voltage (∼20kV) so as to post accelerate the $\bar{p}$s to energies up to 20 keV.

The estimated signal would be

$$N = \sigma n l N_{\mathrm{proj}} = 0.5 \times 10^{-16}\mathrm{cm}^2 10^{12}\mathrm{cm}^{-3} 1\mathrm{cm} N_{\mathrm{proj}} = 5 \times 10^{-5} N_{\mathrm{proj}}$$

which with 1 million $\bar{p}$s extracted from MUSASHI each 5th AD shot or in total 8 million per hour, would give a signal of 400 per hour. This would leave ample room for loss of transmission of the antiprotons into our target region.

Unfortunately, it was not possible to obtain an extracted beam from the MUSASHI trap of intensities near those anticipated in 2003, and we were not able to perform our experiment.

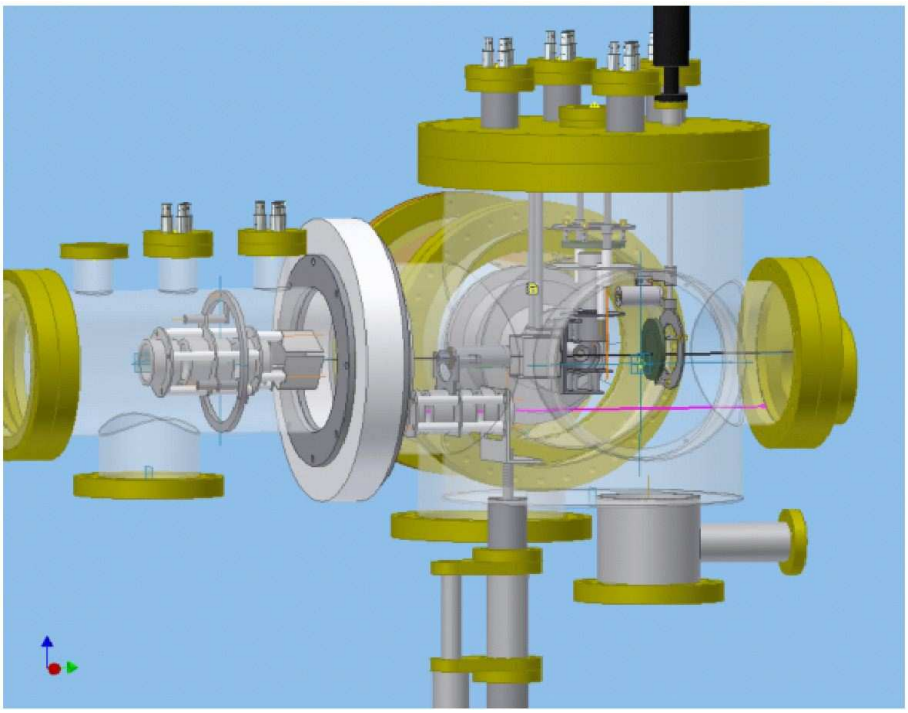

Figure 10: The AIA apparatus.

Instead we "gave" our beam time that year to the trap group for them to use on extraction development. Fearing a negative outcome of the difficult extraction development, we used 2003 to rebuild our apparatus to be able to perform a a fallback version of the experiment in 2004: We built an electrostatic deflector which takes the RFQD beam directly, and selects an energy bin of ∼10%. This is then transported to our target region. This means that we would not have to raise the target to high voltage, but it also meant that our $\bar{p}$ would arrive in bunches ∼200 nsec long. This makes it impossible to measure the TOF of each $\bar{p}$-ion pair, and only a rough TOF of the ions based on the timing signal of the AD can be obtained. Furthermore, it is not possible to detect the number of antiprotons, and only a signal proportional to their number can be obtained from our "end" channelplate running in current mode. Hence this measurement hinges on a comparison between the signal measured at ∼20 keV and the signal measured at lower energies. This would introduce more uncertainty into our measurements, but they are still possible, since the cross section for single ionization has already been measured at 20 keV, see Fig.l 11.

Since, with this method, it is not possible to accept more that ∼0.1 event per AD pulse, we asked the AD technicians to develop a multipulse-ejection, so that each AD pulse could be extracted in 3 or 6 bunches with some seconds interval.

3.2 Status report from our spring run.

Out of 22 beam shifts allotted to our experiment, we had beam only during 12 shifts. This was mainly due to the problems with the AD electron cooler. We found the multi-pulse ejection to work well. We used (as foreseen) 4-5 of the available shifts to tune the beam. However, for the rest of the shifts, we found beam steering and optimization still to be troublesome, since

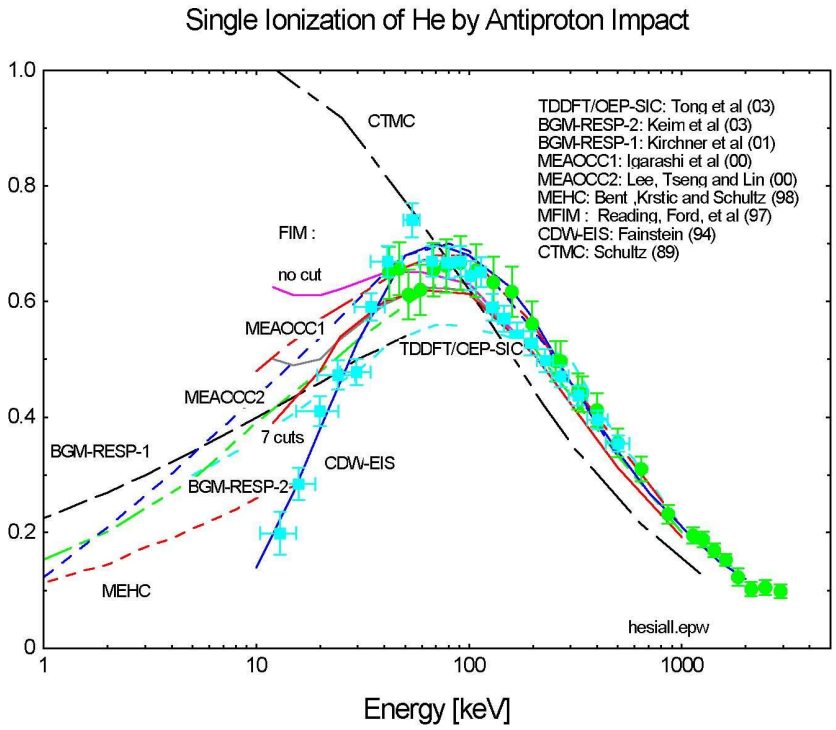

Figure 11: Single ionization cross section of helium by antiproton impact.

apparently the AD parameters changed from shift to shift. We typically used half of a shift for beam tuning. Nevertheless, we were able to collect data for 20 keV $\bar{p}$ on He and Ar, as well as develop beam steering for 10 keV $\bar{p}$.

Figure 12 shows an example of the TOF data obtained for 20 keV $\bar{p}$ on He during 3 hours of beam time. The line is a fit to the data, including a background, which as can be seen is large. We believe this is due to ions created by pions, which are created near the target region by the many $\bar{p}$s that were filtered by the analyzer, but still were dumped near the central part of our apparatus. Nevertheless, we can observe two peaks, one for He^+ and one for He^{++}. They are at the correct TOF positions. Furthermore, the ratio He^{++}/He^+ is 20%, where from an earlier measurements we expected ~50%. So this is reasonable within the large uncertainty of the data. Repeating this measurement, we found a spectrum of the same shape. In total we obtained 29 He^+ during 100 AD cycles, or 3 hours. Assuming the earlier measured cross section, we infer that we got 6000 $\bar{p}$s through our target per AD spill.

3.3 Status report from our autumn run.

A quite new and very satisfying MUSASHI development has been achieved during the summer of 2004, which has been able to extract, to the end of the extraction beam line, a low energy $\bar{p}$ beam. It is extracted each 3 AD spills, is 10 sec long with DC structure, and an energy of 250 eV. It contains up to 5×10^5 $\bar{p}$. The beam-spot at the extraction focus is believed to be 1 cm. This is approximately what was anticipated in the original design of our apparatus. Please note that the post acceleration into our system with at least a factor 10 in energy will improve the beam divergence and radius.

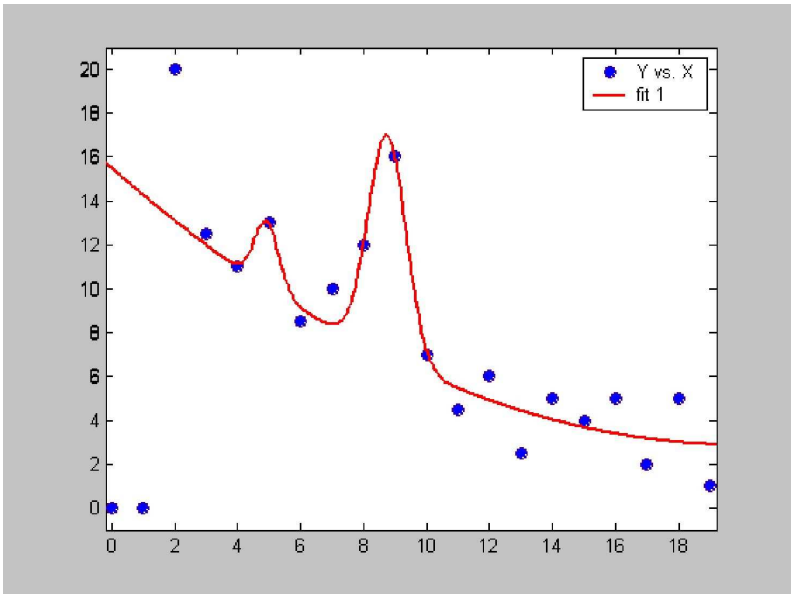

Figure 12: TOF spectrum showing He^{+} and He^{++} peaks.

It was decided to use the extra beam time available to the collaboration for a combined effort to:

1. Establish and further develop the extraction from the trap into our AIA apparatus.
2. To measure ionization cross sections with AIA
3. To measure $\bar{p}$-atom formation.

Unfortunately, a recurring blockage of the cooling loops of the superconducting magnet of the trap caused a great deal of loss of beam time. Nevertheless, extraction into our apparatus was obtained. We were able to get typically 6×10^4 antiprotons per spill onto our $\bar{p}$ detector. We had what amounts to 3 shifts of effective beam time. After that, the blockage happened again, from which we were unable to recover by the end of the 2004 beamtime.

During our beamtime, we obtained TOF spectra for 25 keV $\bar{p}$ with and without He gas in the target cell, as well as a spectrum obtained with 10 keV $\bar{p}$. One spectrum is typically obtained during one shift, due to the time it takes to tune the extraction after the use by other experiments of the $\bar{p}$ beam.

The spectrum, which is shown in Fig. 13 was obtained with 3.88×10^6 $\bar{p}$s passing the gas cell. The other spectra have been renormalized to this number of antiprotons to facilitate a comparison.

As can be seen in the spectra, there is a large background with broad features. It seems to be independent of the target pressure. The origin of this background is not understood at this time. Most $\bar{p}$ annihilation products are emitted from the annihilation site instantly, which should only give added signal in the "prompt" peak around channel 1880. However, muons could be a source of the background, and we will investigate this.

In spite of this background, we are able quite clearly to observe the narrow peak stemming from single ionization of helium atoms in Fig. 13 (channel 1600). This peak is absent in the "no-gas" background spectrum shown in Fig. 14, and is shown in an expended view in Fig. 16.

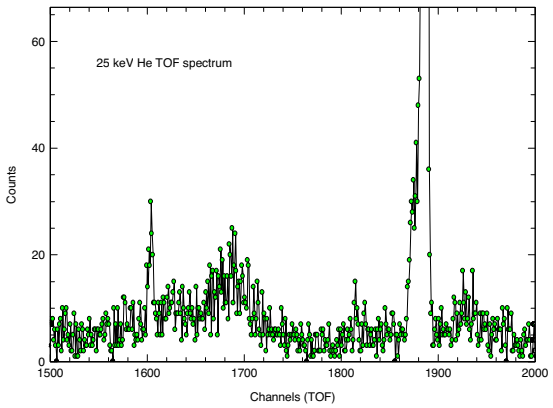

Figure 13:

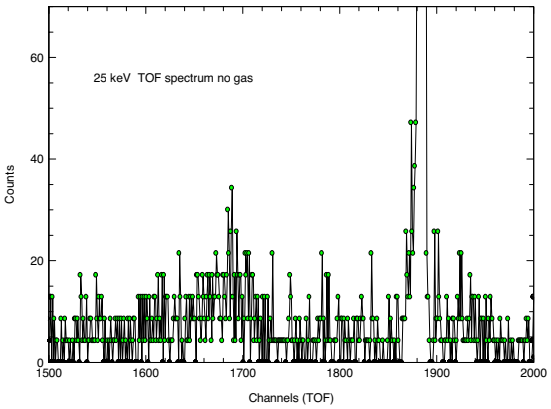

Figure 14:

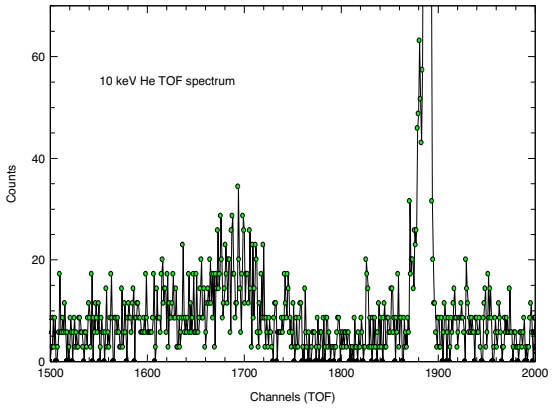

Figure 15:

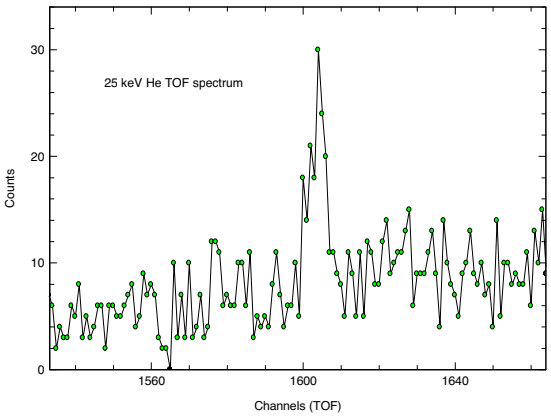

Figure 16:

The associated cross section will be deduced after a re-calibration of the gas density has been performed with the built-in electron beam.

At this time we may, however, point to a very interesting result, namely the absence of a He^+ peak in the 10 keV spectrum. Since the spectra in Figs. 13 and 15 were obtained at approximately the same target pressure, a simple evaluation gives an upper limit of the magnitude of the single ionization cross section at 10 keV of 0.2 times the cross section at 25 keV, or 0.1 $Å^2$ (2σ).

This upper limit seems to agree with the trend of our data measured previously at LEAR (see Fig. 16). If true, this upper limit and our earlier data bring in question all the theoretical calculations published recently! It is worth noticing that the present upper limit and our previous data were obtained with quite different apparatus.

The present situation is shown in Fig. 17:

As seen from the above, we have been able to get quite close to publishable results for the cross section for single ionization of helium, given a few days with a good extracted beam. The cross sections for ionization of atomic hydrogen, neon, argon, etc are approximately an order of magnitude larger than that for helium.

Furthermore, since we did not expect to be able to measure on atomic hydrogen during the autumn run, we removed the Teflon baffle on the gas nozzle. This baffle is designed to prevent ions and UV radiation to reach the target region from the hydrogen discharge, and to "focus" the gas atoms on the target region. The reasoning behind the removal of the baffle was that a

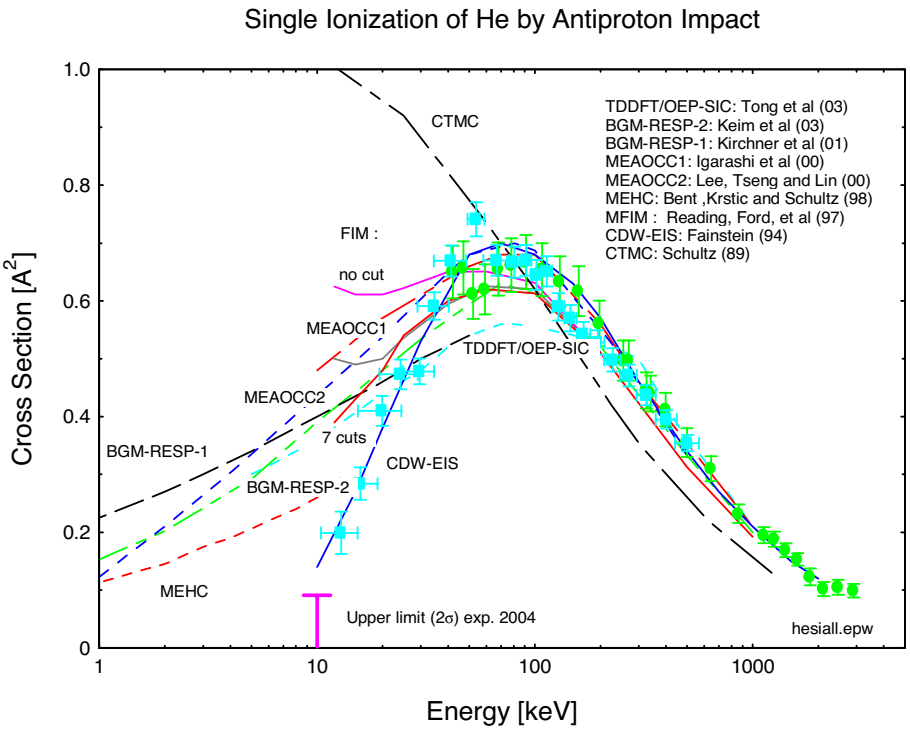

Figure 17: Same as Fig. 11, but with the 2004 PRELIMINARY result added.

higher gas density should be reached. However, we found that we could only reach a gas density 15% of that obtained with the baffle. Using the baffle in our next run, therefore a factor 7 higher signal rate can be expected.

In conclusion, given approximately one month of beam time in 2006, we can obtain comprehensive data on the total cross sections for ionization of atoms by slow antiproton impact with the present setup.

References

[1] M. Hori, J. Eades, R. S. Hayano, T. Ishikawa, W. Pirkl, E. Widmann, H. Yamaguchi, H. A. Torii, B. Juhász, D. Horváth, and T. Yamazaki, Phys. Rev. Lett. 91 (2003) 123401.

[2] S. Eidelman et al., Phys. Lett. B 592 (2004) 1.

[3] R. Holzwarth, T. Udem, T. Hänsch, J. Knight, W. Wadsworth, and P. Russell, Phys. Rev. Lett. 85 (2000) 2264.

[4] T. Udem, R. Holzwarth, and T. Hänsch, Nature 416 (2002) 233.

[5] M. Hori et al., Optics Letters 28 (2003) 2479.

[6] V. Meyer et al., Phys. Rev. Lett. 84 (2000) 1136.

[7] V. I. Korobov, Phys. Rev. A 67 (2003) 062501.

[8] Y. Kino, M. Kamimura, and H. Kudo, Nucl. Instrum. Methods Phys. Res. B 214 (2004) 84.

[9] H. A. Torii, M. Hori, T. Ishikawa, F. E. Maas, R. S. Hayano, N. Morita, M. Kumakura, I. Sugai, B. Ketzer, H. Daniel, F. J. Hartmann, R. Pohl, R. Schmidt, T. von Egidy, D. Horvath, J. Eades, E. Widmann, and T. Yamazaki, Phys. Rev. A 53 (1996) R1931.

[10] P. J. Mohr and B. N. Taylor, to appear in Review of Modern Physics **76** (2004); also available on web at http://physics.nist.gov/constants.

[11] ASACUSA 2003 status report, CERN/SPSC 2004-003, SPSC-M-711.

[12] N. Kuroda, K. Yoshiki Franzen, H. A. Torii, M. Inoue, M. Hori, H. Higaki, A. Mohri, K. Komaki, and Y. Yamazaki, Phys. Rev. Lett., in press.

[13] K. Franzen, N.Kuroda, H.A.Torii, M.Hori, Z.Wang, H.Higaki, S.Yoneda, B.Juhasz, D.Horvath, K. A.Mohri, and Y.Yamazaki, Rev.Sci.Instrum. 74 (2003) 3305.